Li *et al. Environmental Sciences Europe* (2023) 35:114
https://doi.org/10.1186/s12302-023-00821-5

Environmental Sciences Europe

RESEARCH

Open Access

Biogeochemical behavior, health risk assessment and source identification of antimony and arsenic in soil from a legacy antimony smelter in Gansu, Northwest China

Qiang Li[1], Ying Cao[1*], Tian Meng[1], Liansheng He[1] and Sen Zhang[1,2]

Abstract

The study of the contamination patterns and characteristics of Sb and As in the soils of the legacy contaminated sites of antimony smelters is important for the redevelopment and utilization of industrial sites. In this study, 13 heavy metals were determined in the soil and plants of an antimony smelter in Gansu Province to study the biogeochemical behavior, health risk, and pollution source. The results showed that the Nemerow index of Sb (728) exceeded the value of As (43.6) by 17.6 times, and the average geoaccumulation index (I_{geo}) of Sb and As were 10.1 and 1.97, respectively, categorized as extremely and moderately contaminated classes. Compared to As, Sb had a larger proportion of oxidizable fraction and a smaller proportion of reducible fraction (Fe/Mn oxides), suggesting that Sb possessed a higher content of organic matter and sulfide forms. Even though the bioaccumulation factor (BAF) for As was about 10 times higher than that for Sb, the accumulation of Sb in plants was not negligible. For the USEPA model, the mean hazard quotient (HQ) values of As by oral ingestion, dermal absorption, and inhalation accounted for 99.0%, 0.97%, and 0.0002% of the total, and 54.2%, 45.3%, and 0.51% for MEEPRC model, respectively. There were significant positive correlations between Sb, As, Zn, Se, Cd, and Ba ($P < 0.05$). The results of the source identification analysis revealed that antimony smelting, solid waste pollution, and natural origin were identified as the main pollution sources. The principal component analysis (PCA) and positive matrix factorization (PMF) methods differed by more than 20% in the analysis of the contribution of antimony smelting activities and solid waste pollution sources, suggesting the differences in the models themselves and in the uncertainty parameters chosen during the application.

Keywords Antimony smelter, Sb, As, biological accumulation, Human health risk, Source analysis

Introduction

As the ninth most mined metal[16], antimony (Sb) has been listed as a priority pollutant of interest by both the European Union and the United States [8, 39]. China is the leading producer of Sb worldwide and Almost 80% of Sb production was concentrated in China, Russia, and Bolivia [2, 21]. China's antimony mine production amounted to approximately 80,000 metric tons in 2020, thus China was the leading producer of antimony in the world. Metal mining, mineral processing, and smelting generated large amounts of emissions, wastewater,

*Correspondence:
Ying Cao
caoying@craes.org.cn
[1] Environmental Testing and Experiment Center, Chinese Research Academy of Environmental Sciences, Beijing 100012, China
[2] North China University of Science and Technology, Tangshan 063210, China

and sludge [54]. These pollutants could enter the soil environment through emissions, leaks, rainfall, sedimentation, diversion, and infiltration [23, 38, 57]. With the continuous discharge of smelter pollutants, heavy metals(HMs) in the soil would continue to enrich and have adverse health effects through the food chain and long-term exposure, thus increasing the risk of chronic poisoning and cancer in humans [22, 25, 46]. With the transformation and upgrading of China's national industrial structure and the further promotion of green and low-carbon development, a large number of highly polluting enterprises located in urban centers had moved out, leaving a large number of abandoned sites [49, 50, 53]. The serious risk of soil contamination at these abandoned sites had led to difficulties in the subsequent redevelopment and utilization of the sites. With the introduction of China's "Action Plan for Soil Pollution Prevention and Control" and "Soil Pollution Prevention and Control Law", a detailed investigation of soil pollution, soil pollution prevention at source, remediation, and risk control projects had been carried out, and soil pollution prevention and control work was getting more and more attention [3].

Similar to arsenic (As), Sb possesses an s2p3 outer orbital electron configuration and thus occurs in the form of (− III, 0, + III, and + V). As an emerging contaminant, Sb has been assumed to have comparable geochemical behavior and toxicity with As. However, when they exist as mixtures, the different coordination structures and interactions between contaminants lead to their different geochemical behavior and biotoxicity under different conditions [7, 47]. Tremendous effort has been devoted to understanding the pollution characteristics, biogeochemical behavior, and ecological risk of Sb and As pollution [36, 55, 56], whereas research specific to source identification of Sb in the soil inside an antimony smelter is limited. In China, studies on soil contamination in antimony mines were mainly focused on two areas, such as Xikuangshan antimony mine in Hunan Province and the Qinglong antimony deposit in Guizhou Province [17, 34]. Most studies focused on the pollution of surrounding agricultural soils by smelters [1, 20, 56] or in the lab [6, 30], and the research objects were limited to certain elements such as Sb, and there were few systematic studies on the contamination characteristics, biogeochemical behavior, health risks and sources of highly contaminated soils inside antimony smelters.

Longnan City, Gansu Province, had large, high-grade mineral reserves, including 149,000 tons of antimony metal reserves, accounting for 8% of China, and its reserves ranked third in the country. An antimony smelter in Longnan City had a production history of nearly 30 years and had production lines for mining, beneficiation, and smelting at the same time, with the main products being antimony concentrate powder and refined antimony. In this study, thirteen HMs, including Sb and As, were determined in the soil of an antimony smelter, hoping to provide technical support for the prevention of soil pollution and utilization of antimony smelting industry sites. The human health risk was evaluated using two models from USEPA and MEEPRC, and the sources of HMs were analyzed using correlation analysis, PCA, and PMF. This study will increase our knowledge about pollution characteristics, biogeochemical behavior, health risk assessment, and source identification of antimony and arsenic in similar antimony-smelting-affected soils and utilization of different models.

Materials and methods

Sampling sites and sample collection

The study area, the antimony smelter, is situated between 30.0°N and 105.3°E in Xihe County, Longnan City, in the south of Gansu Province. The antimony smelter was founded in 1986 and ceased production in 2013, mainly engaged in antimony smelting. The antimony reserves of the antimony mine belonging to the antimony smelter ranked third in China and first in the Northwest. The company's main product was refined antimony, with an annual output of 3000 tons. The area is in the Longnan Mountains, with elevations ranging from 1560 to 2157 m. The smelter is located on the west side of the river, surrounded by residential areas, agricultural land, schools, drinking water wells, etc.

A total of 20 sampling points were collected considering the distribution of antimony smelting workshops, material, and waste storage areas, as well as the contamination traces at the site(Additional file 1: Fig. S1). At each sampling point, fresh soil was collected from the surface layer (at a depth of 0 ~ 20 cm), 3 ~ 5 sub-samples were collected at each sampling point, and 1kg of soil samples were taken into polyethylene bags after mixing. The mugwort plants were also collected at six points, and the leaves, stems, and roots were intercepted and preserved in sample bags. Finally, all samples were stored in ice-packed coolers and immediately transported to the laboratory.

Sample analysis and quality control

All soil samples were transported to the laboratory and other objects such as sticks and stones were removed. Then they were naturally dried, ground, and passed through 10 and 100-mesh nylon sieves for testing. The plant samples were rinsed individually with tap water and deionized water to remove possible metal contaminants. Then they were

dried and the leaves, stems, and roots were homogenized separately and evenly. The total amount of thirteen elements in soil samples and plant samples was determined with two standards [28, 29, 32], using a microwave digestion instrument (CEM Mars 6, USA) for digestion and an inductively coupled plasma mass spectrometer (ICP-MS, Agilent 7800, USA) for determination.

The BCR sequential extraction procedure is used in studying the chemical fractionation of the in the soils, before and after exposure [37]. The modified BCR (European Community Bureau of Reference) procedure was carried out with four steps: Step1-exchangeable, water- and acid-soluble fraction (F1), 0.11mol·L^{-1} CH_3COOH; Step2-reducible fraction (F2), 0.5mol/L NH_2OH•HCl at pH 2; Step3-oxidisable fraction (F3), H_2O_2 (85 ℃) then 1 mol/L CH_3COONH_4; Step4-residual fraction (F4) corresponding to the total digestion. All reagents used were pure grade.

The analytical process was subjected to strict quality control, including method blanks, sample duplicates, and matrix spiking. The correlation coefficients of the standard curves for the HM samples were all greater than 0.999, and the method blanks were lower than the detection limits or less than 10% of the lowest determined values of the samples. The relative deviations were all less than 13.9% for soil duplicates, 11.7% for plant duplicates, and 18.1% for soil duplicate samples extracted by the BCR procedure. The recoveries of matrix spiking for soil samples ranged from 98.2 to 120%, and those for plant samples ranged from 78.8 to 106%. All samples with outliers were analyzed again by repeating the standard procedure.

Assessment of the HM pollution

Single pollution index (PI) and Nemerow integrated pollution index (P_N) were used to evaluate the level of HM pollution [13] as follows:

$$P_i = \frac{C_i}{S_i} \tag{1}$$

$$P_N = \sqrt{\frac{(P_{\text{imax}})^2 + (P_{\text{imean}})^2}{2}} \tag{2}$$

where P_i is the single pollution index; C_i is the measured concentration of a single HM (mg·kg^{-1}); S_i is the standard value for the evaluation (mg·kg^{-1}); P_N is the Nemerow index; P_{imax} is the max value of single pollution index; P_{imean} is the average vales of single pollution index. The Nemerow index (P_N) has five classifications: $P_N \leq 0.7$ indicates excellent; $0.7 < P_N \leq 1.0$ indicates clean; $1.0 < P_N \leq 2.0$ indicates slightly polluted; $2.0 < P_N \leq 3.0$ indicates moderately polluted; $P_N > 3.0$ indicates heavily polluted [48, 52].

I_{geo} was used to estimate the anthropogenic pollution of metal concentration enrichment above background concentrations [31]:

$$I_{\text{geo}} = \log_2\left[\frac{C_n}{1.5\,B_n}\right] \tag{3}$$

where C_n is the metal concentration in the enriched samples, the factor 1.5 is introduced to minimize the effect of possible variations in background concentrations at the site, and B_n is the background concentration of the element. Results obtained are classified into descriptive classes for increasing I_{geo} values. The geoaccumulation index has seven classifications: $I_{geo} \leq 0$ indicates uncontaminated, $0 < I_{geo} \leq 1$ indicates slightly contaminated, $1 < I_{geo} \leq 2$ indicates moderately contaminated, $2 < I_{geo} \leq 3$ indicates moderately heavily contaminated, $3 < I_{geo} \leq 4$ indicates for heavily contaminated, $4 < I_{geo} \leq 5$ indicates extremely heavily contaminated and $I_{geo} > 5$ indicates extremely contaminated[17].

Health risk assessment model

Human health risk assessment was estimated through three main pathways, ingestion, dermal, and inhalation absorption, using two different methods from USEPA and MEEPRC [27, 40–42]. The average daily dose (ADD) of HM exposure from the MEEPRC method was estimated using equations [27]:

$$ADD_{ing} = \frac{C \times IR_{ing} \times ED \times EF}{BW \times AT} \times 10^{-6} \tag{4}$$

$$ADD_{der} = \frac{C \times SA \times AF \times ABS \times EF \times ED}{BW \times AT} \times 10^{-6} \tag{5}$$

$$ADD_{inh} = \frac{C \times PM_{10} \times IR_{inh} \times ED \times PIAF \times (fspo \times EFO + fspi \times EFI)}{BW \times AT} \times 10^{-6} \tag{6}$$

The definitions and values of these parameters are listed in Additional file 1: Table S1, where C is the concentration of HMs in soil. Non-carcinogenic risk (HI) and carcinogenic risks (CR) for all metals by three exposure routes were calculated using the following equations:

$$HQ_i = \frac{ADD_i}{RfD_i \times SAF} \tag{7}$$

$$HI = \sum HQ_i \tag{8}$$

$$CR = ADD \times SF \tag{9}$$

where HQ_i is the hazard quotient of the metal i; RfD_i is the reference dose of the metal i ($mg \cdot kg^{-1} \cdot d^{-1}$); SAF is the soil allocation factor and the value of metals is 0.5; SF is carcinogenicity slope factor ($mg \cdot kg^{-1} \cdot d^{-1}$). Values of RfD and SF of metals were listed in Additional file 1: Table S2. The acceptable level for non-carcinogenic risk is < 1 and the value of CR should not exceed 1×10^{-6}. For CR, 1×10^{-4} to 1×10^{-6} is the acceptable or tolerable risk range, and there is a potential carcinogenic risk if $CR > 1 \times 10^{-4}$ [19, 43].

Positive matrix factorization

Positive matrix decomposition (PMF) was a modified factor analysis receptor model for source assignment proposed by Paatero and Tapper [35]. The concentration data could be viewed as a data matrix, which could then be decomposed into two matrices, including the factor contribution (G) and the factor distribution (F).

$$x_{ij} = \sum_{k=1}^{p} g_{ik} f_{kj} + e_{ij} \tag{10}$$

where x_{ij} is the concentration matrix of the j-th HM in the i-th sample, g_{ik} is the concentration matrix of the k-th source to the i-th sample, f_{kj} is the characteristic value of the j-th HM concentration of the k-th source, and e_{ij} is the residual matrix of samples.

Factor contributions and profiles can be determined by using the minimum value of the objective function Q in the following formula:

$$Q = \sum_{i=1}^{n} \sum_{j=1}^{m} \left(\frac{e_{ij}}{u_{ij}} \right)^2 \tag{11}$$

where u_{ij} is the uncertainty of the j-th HM in the i-th sample.

If the HM concentration does not exceed the method detection limit (MDL) value, then the value of the uncertainty is equal to 5/6 MDL, otherwise, it is calculated as follows [9]:

$$u_{ij} = \sqrt{MDL^2 + (Error\,fraction \times C)^2} \tag{12}$$

where C is the concentration of the HMs and the Error fraction is the error rate [10].

Statistical analyses

Statistical analysis of the data was completed using Microsoft Excel 2016 and Originlab 2021. Spatial analysis and variability were performed in ArcGIS 10.2 (Esri Inc., USA) using the inverse distance weight method. Spearman's correlation analysis and principal component analysis (PCA) were performed using SPSS Statistics 20 software (IBM Inc., USA), and source identification analysis was performed using the PMF 5.0 software (USEPA, USA).

Results and discussion

Descriptive statistics of HMs in soils

Basic statistical parameters of the total concentrations of HMs in Sb smelting industry sites were summarized (Table 1). The maximum values of HMs that exceeded the risk screening values were Sb, As, Zn, and Pb, and

Table 1 Statistical analysis and pollution evaluation of HMs concentrations in soils/$mg \cdot kg^{-1}$

Element	Sb	As	Cr	Co	Ni	Cu	Zn	Se	Mo	Ag	Cd	Ba	Pb
Minimum	148	15.7	40.6	9.64	25.0	22.5	63.5	3.64	0.27	0.12	0.09	201	24.9
Median	1.62×10^3	53.8	49.1	13.6	40.0	38.2	369	10.9	1.20	0.80	1.91	245	169
Maximum	1.85×10^5	3.69×10^3	95.5	45.0	162	523	1.68×10^4	1.70×10^3	14.0	19.1	44.8	723	5.50×10^3
Mean	1.66×10^4	319	53.0	19.6	61.3	85.5	1.78×10^3	138	3.52	3.66	4.71	323	692
SD	4.29×10^4	833	14.7	11.9	40.5	115	3.79×10^3	393	4.20	5.38	9.82	162	1.33×10^3
CV	258%	261%	27.8%	60.7%	66.1%	134%	213%	285%	119%	147%	208%	50.0%	192%
Risk screening values[a]	180	60	2000	70	900	18,000	2000	800	700	/	65	2000	800
Soil background values[b]	1.26	12.6	70.2	12.6	35.2	24.1	68.5	/	0.8	0.132	0.116	446	18.8

a Risk screening values are the soil quality standard values for soil contamination of industrial land in China's soil environmental quality standard [4, 26]

b Soil background values are soil element background values in Gansu province [5]

the maximum values of all 12 HMs exceeded the soil background values. The coefficient of variation (CV) of HMs more than 200%, in descending order, were Se, As, Sb, Zn, and Cd, and the HMs with CV less than 100%, in descending order, were Ni, Co, Ba, and Cr. Among them, only Sb and As exceeded the risk screening values in terms of their arithmetic mean values, suggesting potential health risks. The concentration of As in background soils was almost 10 times that of Sb, but the average concentration of Sb in soils in Sb mining areas was 52 times that of As. The mean concentrations of Sb and As exceeded risk screening values by 92.2 and 5.3 times. The maximum concentration values of Sb and As were 1250 and 235 times greater than the minimum concentration values.

The single pollution index of Sb and As was $0.82 \sim 1.03 \times 10^3$ and $0.26 \sim 61.5$ (Additional file 1: Fig. S2). Approximately 95% single pollution index of the sampling points exceeded 1, while the percentage of As was 40%. HM in the soil was considered heavily contaminated when the Nemerow index (P_N) > 3, while the values of Sb (728) exceeded the values of As (43.6) by 17.6 times. In addition, P_i values of Sb and As in different points are similar in distribution, suggesting identical spreading trends and pollution sources. All I_{geo} of the soil samples for Sb exceeded 5, indicating that all sampling points were extremely contaminated (Additional file 1: Fig. S3). For As, I_{geo} of two sampling points exceeded 5, and three of them were under 0. The average I_{geo} values of Sb were 10.1, categorized as an extremely contaminated class. In contrast, the average I_{geo} values of As were 1.97, categorized as a moderately contaminated class.

Biological accumulation of Sb and As in soils

The proportions of each HM chemical form in the 20 soil samples are shown in Fig. 1. In descending order, the HMs with a high proportion of residual fractions were Cr, Cu, As, Sb, and Pb, and those with a high proportion of F1 + F2 + F3 were Cd, Se, Zn, Ba, and Co. Among the sites, the proportion of F1 + F2 + F3 was relatively high at site S17. As for Sb and As, most of them were bound in residual fractions, some of them were in

Fig. 1 Chemical speciations of Sb and As in 20 soil samples

the reducible and exchangeable fractions, and very few of them were in the oxidizable fraction. Compared to As, Sb had a larger proportion of oxidizable fraction and a smaller proportion of reducible fraction, suggesting that Sb possessed more organic matter and sulfide forms, while As possessed more iron-manganese oxide forms. After a simple calculation, the F1 + F2 + F3 ratios of Sb and As at some points were relatively high, with the maximum values being 32.0% and 23.5% at point S17, respectively. The F1 + F2 + F3 ratios of Sb and As at some points were relatively low, with the minimum values being 1.0% at point S5 and 0.45% at point S20, respectively. Compared to As, the F1 ratio of Sb was generally higher, with the mean values of Sb and As being 6.4% and 3.9%, respectively. The sampling sites with F1 values over 10% for Sb were S8, S11, S16, and S17, while the sites with F1 values over 10% for As were S4 and S17, respectively. The maximum F1 values of Sb and As were 19.1% and 11.3% at point S17, respectively.

The calculated bioaccumulation factor (BAF i.e. organism/soil concentration ratios to estimate the bioavailability) for As were about 10 times higher than those for Sb, and similar results were obtained for Chemical fractions (F1 + F2 + F3) (Additional file 1: Fig. S4). Even though the BAF values of Sb were much smaller than those of As, the mean BAF values of Sb total contents in soils still exceeded 10, indicating that the accumulation of Sb in plants was not negligible. Both elements tended to be less accumulated in stems than in other parts. The order of BAF values for As was root > leaf > stem, while the order of BAF values for Sb was leaf > root > stem. And the order did not change in the results of chemical fractions. Previous studies showed that Sb accumulated more in leaves than in roots in other antimony smelting regions [11, 15].

Organic matter was positively correlated with total Sb and negatively correlated with BAFs of Sb (Fig. 2). pH was the opposite, but pH was less correlated with the BAFs of Sb. Positive correlations between BAFs of Sb and pH were in agreement with the previously reported results [14]. Both total contents and chemical fractions of Sb had a strong correlation with organic matter and pH, and the absolute value of the correlation coefficient all exceeded 0.97. The results of the correlation of As with organic matter and pH showed no obvious regularity, except for the BAFs of stems. At levels of Sb content between 250 and 5000 mg·kg^{-1}, the total Sb was negatively correlated with the BAFs of Sb, indicating that the increase of the total Sb would weaken the mobility of Sb. Although Sb pollution would not cause a sharp increase in the bioavailable levels, the high content of Sb in soils would still lead to an increase in the bioavailable content of Sb. In contrast, at levels of As content between 10 and 100 mg/kg, the total As was positively correlated with the BAFs of As, indicating that the increase in the total amount of As would enhance the mobility of As. There were strong positive correlations between the three BAFs of Sb, while the strong correlation of arsenic existed only between roots and leaves. There were also strong positive correlations between the three BAFs of Sb and the two BAFs of As. However, for total contents in soils, the BAFs of As were statistically different from the two BAFs of Sb ($p \leq 0.05$). Overall, the BAFs of As were significantly higher than those of Sb, and the increase in soil As content might simultaneously lead to increased bioaccumulation in the roots, stems, and leaves of plants. Although

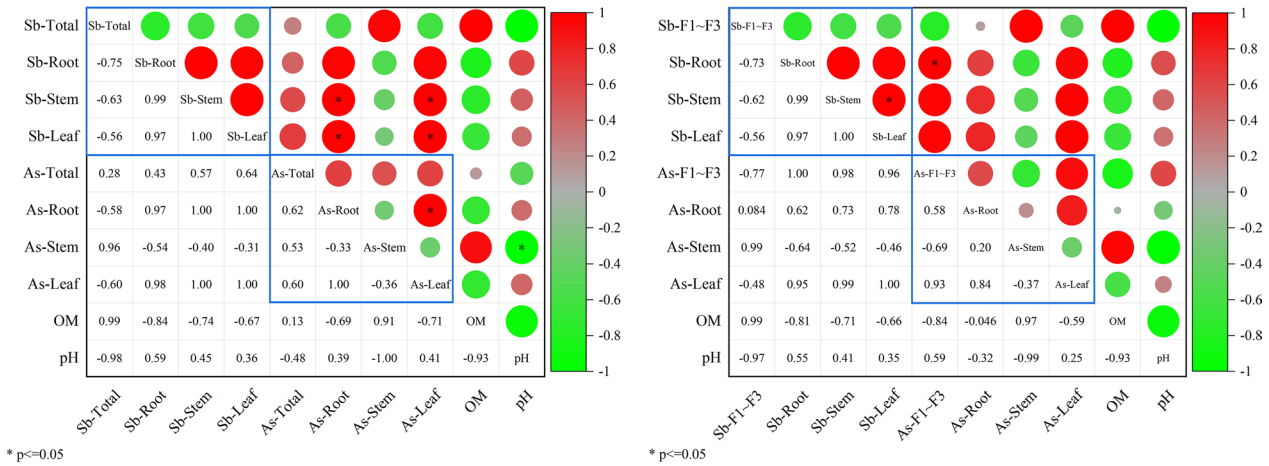

Fig. 2 Correlations between organic matter, pH, soil concentration and BAFs of As and Sb in mugwort plants: **a** Total contents in soils, **b** Chemical fractions (F1 + F2 + F3) in soils

the BAFs of Sb were relatively low, the high Sb content in soil still led to an increase in the bioavailable level of Sb, which should be of concern.

Health risk assessment

Since the sampling points were all in the internal area of the antimony smelter site and the sampling area was limited, this risk assessment focused on analyzing the human health risk of smelter workers and provided an important basis for whether the antimony smelter could be safely utilized. Non-carcinogenic and carcinogenic risks of HMs in soil were calculated using the MEEPRC model (Additional file 1: Fig. S5). HMs with HQ mean values exceeding 1 were Sb and As, indicating an unacceptable non-carcinogenic risk. The mean HQ values were close to 100 for Sb, less than 10 for As. HMs with CR mean values exceeding 1×10^{-6} were As and Pb. The mean CR values were more than 1×10^{-4} for As, indicating there was a potential carcinogenic risk.

The hazard quotient of Sb and As via oral ingestion, dermal absorption, and inhalation for children and adults were calculated using two different models from USEPA and MEEPRC (Additional file 1: Fig. S6). The shape of Sb was highly similar between the two different models, as was the shape of As, indicating that the results of HQ varied mainly with elemental content under fixed conditions of exposure pathway, land type, and population type. For oral ingestion, HQ values of Sb for most samples and As for a small percentage of samples exceeded 1, indicating an unacceptable level of risk for adverse health effects. For adults, the mean HQ values of Sb and As were over 57 and 1.45, while the maximum values of Sb and As were 1020 and 27.2, respectively. For inhalation, HQ values for both models were less than 1, indicating that the human health risk was acceptable. For the EPA model, the mean HQ values of As by oral ingestion, dermal absorption, and inhalation accounted for 99.0%, 0.97%, and 0.0002% of the total, and 54.2%, 45.3%, and 0.51% for the MEE model, respectively. The differences between the two models were mainly due to the differences in parameters and some of the calculation equations, and the MEE model took fully into account the characteristics of industrial sites. However, the MEE model was conservative in the selection of parameters, resulting in significantly higher health risks than the results of the EPA model.

For adults, the hazard quotient results of the MEE model were generally higher than those of the EPA model, especially for inhalation, and dermal absorption. For oral intake, the difference between the two models was not significant, because the average body weight of the MEE model was lighter, which was the reason for the high HQ value of the MEE model. For dermal absorption, the HQ values of the MEE model were significantly higher than those of the USEPA model. Because the skin adherence factor in the MEE model was adjusted from 0.07 to 0.2 to account for the industrial site scenario. And dermal absorption factor for As in the MEE model was 30 times higher. For inhalation, the MEE model took into account the higher PM_{10} and indoor-outdoor exposure scenarios, resulting in much higher results from the MEE model than from the EPA model. For the USEPA model, the HQ values of children were higher than those of adults, except for inhalation.

Due to the high proportion of residual fraction of Sb and the low bioaccumulation factor, using the total amount of Sb for the calculation would exaggerate its health risk, so the health risk assessment was carried out using fractions F1, F2, and F3. The hazard quotient of total contents and chemical fractions (F1 + F2 + F3) of HMs via oral ingestion for adults were calculated using the MEE model (Fig. 3). For both Sb and As, the results for total contents and chemical forms differed significantly. For the total content of Sb, HQ values exceeded 1 at 95% of the points and the maximum value exceeded 1000, indicating an unacceptable health risk. However, for the three chemical forms of Sb, HQ values exceeded 1 at 45% of the points and the maximum value did not exceed 60. For the total content of As, HQ values exceeded 1 at 25% of the points and the maximum value was 27.2. However, for the three chemical forms of As, HQ values exceeded 1 at 5% of the points and the overall picture was green. The figure showed that the risk was higher in the north of the study area and relatively lower in the south, which was because production plants were mainly located in the northern area and offices were located in the southern area. The result of point S16 was too high and differed from the results of surrounding points by hundreds of times, resulting in a reddish surrounding of this point, and there might be a local pollution leakage at this point.

The carcinogenic risks of total contents and chemical fractions of As via oral ingestion and inhalation for adults were calculated using the MEE model (Additional file 1: Fig. S7). For both oral and inhalation, the results for total content and the three chemical forms differed significantly. For the total content of As via oral ingestion, CR values exceeded 1×10^{-4} at 40% of the points and the maximum value exceeded 5×10^{-3}, indicating a potential carcinogenic risk. However, for the three chemical forms of As, CR values exceeded 1×10^{-4} at 5% of the points and the maximum value did not exceed 1×10^{-3}. For the total content of As via inhalation, CR values exceeded 1×10^{-6} at 90% of the points and the overall image was blue, indicating an acceptable or tolerable risk. However,

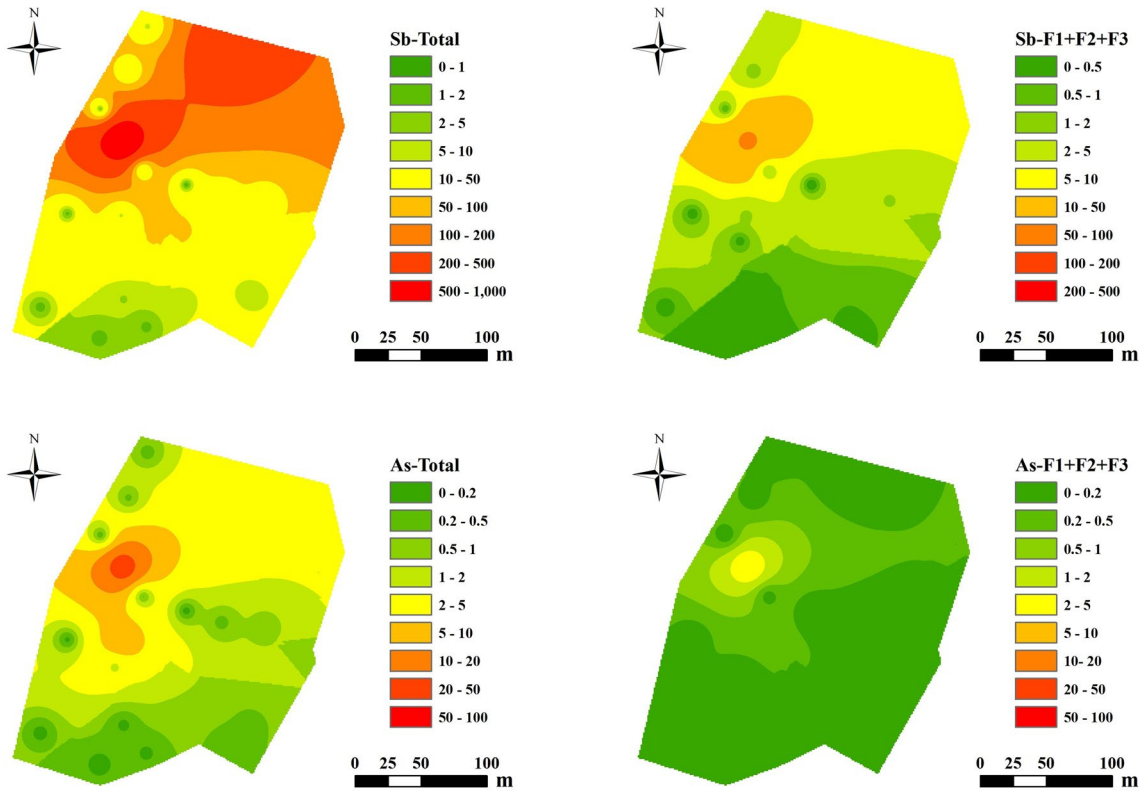

Fig. 3 Non-carcinogenic risk of total contents and chemical fractions of HMs via oral ingestion

for the three chemical forms of As, CR values exceeded 1×10^{-6} at 45% of the points and the overall image was green. The figure showed that the risk was higher in the north of the study area and relatively lower in the south and this result was the same as Additional file 1: Fig. S4. The above results indicated that it was crucial to conduct correlation studies and comprehensive impact assessments in the vicinity.

Source identification

The Spearman correlation coefficients for thirteen HMs in soils showed that most of the elements had a relatively significant correlation and an overall positive correlation (Additional file 1: Fig. S8). There were significant positive correlations between Sb, As, Zn, Se, Cd, and Ba, and the correlation coefficients were all greater than 0.68 ($P<0.05$). The correlation between Sb and As was very significant with a correlation coefficient of 0.91, indicating that they may be derived from the same sources and spreading processes. The correlation between Cr, Co, Ni, Cu, Mo, and Ag and the above elements were insignificant or no correlation, but they had significant positive correlation with each other. The correlation between Ba and other elements was the most significant, while the correlation between Pb and other elements was relatively insignificant.

The KMO value ($0.680>0.5$) and Bartlett's test ($p<0.001$) showed that the samples were suitable for principal component analysis (PCA). Based on the principle of eigenvalues higher than 1, three factors were screened, explaining 95.1% information of the variables (Fig. 4). Factor 1, Factor 2, and Factor 3 explained 49.2%, 36.4%, and 9.5% of the total variance, respectively, reflecting most of the information in the original data. The elements with high loading coefficients for factor 1 (PC1) were mainly Ba, Mo, Zn, Sb, Cd, Pb, As, and Se, all of which had significant positive correlations with Ba. The concentrations of Ba in some soils were higher than the background value in Gansu Province, and elements such as Sb and As were heavily contaminated. All of these elements, including Ba, had relatively high concentrations at points S8, S12, S16, and S20, which were all near the antimony smelting workshop, indicating that the first factor was mainly identified as the antimony smelting source. Smelting activities led to the contamination of Pb, because of Jamesonite ($Pb_4FeSb_6S_{14}$) [33]. Wang et al. [44] also reported that Cd, Pb, and Zn were derived from the sulfide mineralization paragenesis in antimony mines.

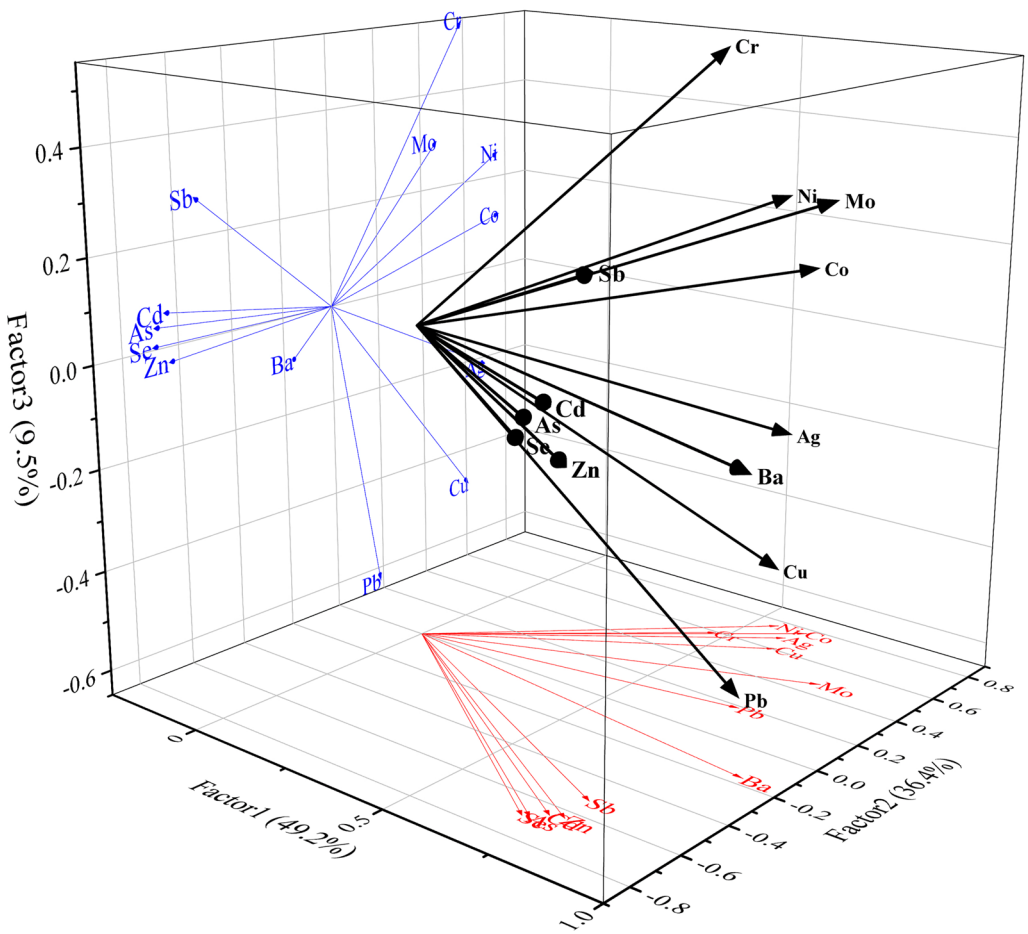

Fig. 4 Loading plot of HMs in soils

The elements with high loading coefficients for PC2 were mainly Co, Ni, Ag, Cu, Cr, and Mo, all of which had significant or certain positive correlations with each other. These elements were relatively less polluted compared to the other elements, and the loadings coefficients of Sb and As in factor 2 were both negative. Most of these elements had relatively high concentrations at points S5, S6, S12, and S13, which were all near the water-quenched slag and desulfurized slag storage workshop, indicating that the second factor was mainly identified as the solid waste pollution source. Water-quenched slag was enriched in Co, Cr, Cu, Ni, and other HMs, and its leakage could lead to soil contamination [12].

The elements with high loading coefficients for PC3 were mainly Cr, Mo, Sb, and Ni, with significant positive correlations between Cr, Mo, and Ni. There were positive correlations between Sb and the other three elements, but the correlation coefficients were small and all were less than 0.41. The highest loadings were observed for Cr (0.546), followed by Mo (0.300) and Sb (0.275). The Cr contents in all samples were close to the background value, and the coefficient of variation was less than 30%, indicating that Cr was less affected by anthropogenic activities. Cr and Ni were mainly attributed to natural factors such as the weathering and leaching of parent materials [24]. Factor 3 was considered to be mainly controlled by background values, indicating that these HMs were mainly derived from natural sources caused by the soil parent material.

To obtain more accurate quantitative information on the contribution of metal sources in soil, the PMF model was used to quantify the main potential source contributions. PCA is generally used to determine the optimal number of factors [45], and "4" was set as the number of sources (Fig. 5). The signal-to-noise ratios (S/N) of all selected elements were greater than 2 and are classified as strong, except for Ag (S/N = 1.3) which is classified as weak. Except for Cu and Pb ($r^2 < 0.6$), the fitting coefficients (r^2) of most elements were greater than 0.75, and the residual values of most elements were between -3 and 3. Based on the above, it indicated that the PMF model results were suitable for interpreting HM source

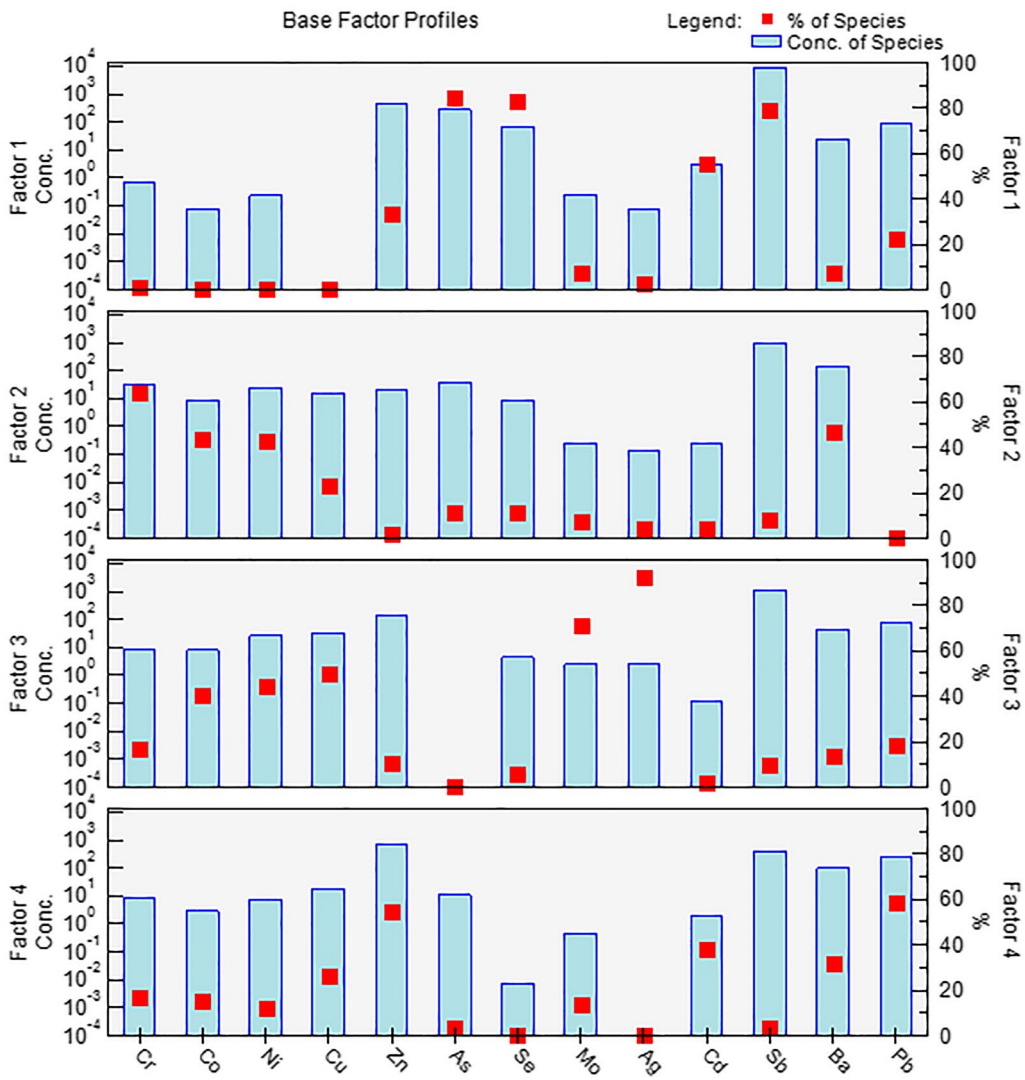

Fig. 5 Factor profiles and source contributions of HMs in the soils based on the PMF

information [18]. The relative contributions of the four factors of soil HMs resolved by the PMF model were 70.2%, 8.9%, 10.2%, and 10.7%, respectively.

Factor 1 was dominated by As, Se, Sb, and Cd, with high loading values of 85.0%, 83.2%, 78.7%, and 55.1%, respectively. The loading values of characteristic pollutants (Sb and As) were high, and the above elements were similar to PC1. Sb, As, and Cd could be attributed to anthropogenic inputs around an antimony mine area [24]. Therefore, factor 1 originated from antimony smelter plant emissions. Factor 2 was dominated by Cr (64.5%), Ba (46.8%), Co (44.0%), and Ni (42.6%), with significant positive correlations between Cr, Co, and Ni. All of them relatively were close to the background values, and the coefficients of variation were less than 66.1%, indicating that they were less affected by anthropogenic activities. Factor 2 was similar to PC3 in the PCA results and represented the natural origin. Factor 3 was dominated by Ag (92.7%), Mo (71.3%), Cu (50.3%), Ni (44.5%), and Co (40.6%), all of which had significant or certain positive correlations with each other. The obtained factor loadings were consistent with PC2 in the PCA results, indicating that factor 3 was mainly identified as the solid waste pollution source. Factor 4 was dominated by Pb (58.9%), Zn (54.4%), Cd (38.1%), and Ba (31.6%), with significant positive correlations between Zn, Cd, and Ba. The concentrations of Pb, Zn, and Cd were high and exceeded the background values, with coefficients of variation greater than 192%, indicating that they were highly affected by anthropogenic activities such as raw material preparation, tail gas absorption, sewage treatment, smelting slag stockpiling, etc.

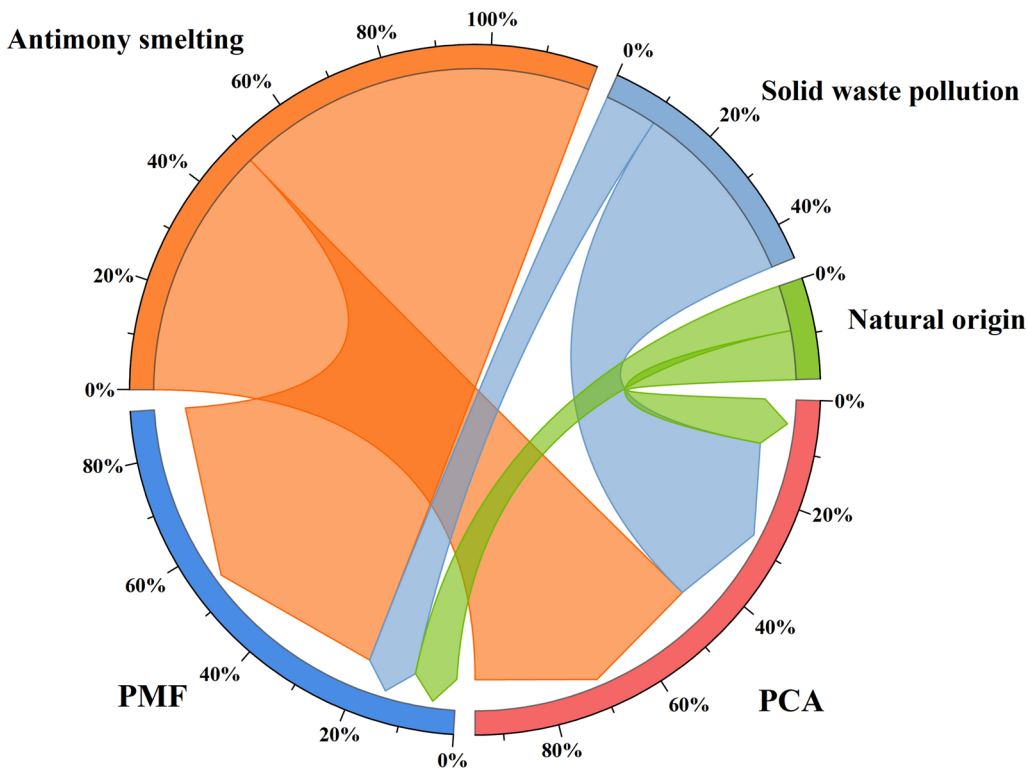

Fig. 6 Source apportionment and contribution rates of PCA and PMF models

The source assignment and relative contribution of the PCA and PMF methods are shown in Fig. 6, with consistent results for contaminated sources. Both methods resolved the sources of antimony smelting activities with high contribution rates of 49.2% and 70.2%, respectively. Solid waste pollution and natural sources were the other 2 sources resolved, and the relative contributions obtained from the analysis were 36.4%, 9.5% (PCA), 10.2%, and 8.9% (PMF), respectively. Natural sources accounted for less than 10% in both models, suggesting that human activities accounted for the majority of the pollution source contribution. This indicated that the main source of soil contamination in the antimony smelter was the 27-year-long antimony smelting industrial production emissions and the historical accumulation and spreading of solid waste. The two methods differed by more than 20% in the analysis of the contribution of antimony smelting activities and solid waste pollution sources. This was mainly due to the differences in the two models themselves and in the uncertainty parameters chosen during the application. In contrast to PCA, PMF took full account of data uncertainty and adopted non-negativity constraints [51]. There were negative values of the principal component loadings, and the PCA analysis results were not proportional to the source contributions, although they were correlated. In contrast, the values in the PMF source component plots were all positive and the fitting coefficients (r^2) of most elements were greater than 0.75, indicating a good correlation between the predicted and observed values of the HM content variables.

Conclusion

In this study, thirteen HMs, including Sb and As, were determined in the soil of an antimony smelter in Gansu Province. Compared to As, Sb had a larger proportion of oxidizable fraction and a smaller proportion of reducible fraction (Fe/Mn oxides), suggesting that Sb possessed a higher content of organic matter and sulfide forms. Even though the bioaccumulation factor (BAF) for As was about 10 times higher than those for Sb, the mean BAF values of Sb total contents in soils still exceeded 10, indicating that the accumulation of Sb in plants was not negligible. Organic matter was positively correlated with total Sb and negatively correlated with BAFs of Sb. pH was the opposite, but pH was less correlated with the BAFs of Sb. These suggested that within a certain range, if the organic matter content decreased and pH increased, it might cause a further increase in the risk of Sb bioaccumulation. For the EPA model, the mean HQ values of As by oral ingestion, dermal absorption, and inhalation accounted

for 99.0%, 0.97%, and 0.0002% of the total, and 54.2%, 45.3%, and 0.51% for the MEE model, respectively. The differences between the two models were mainly due to the differences in parameters and some equations. The MEE model fully considered the characteristics of industrial land, but further optimization was needed in the model parameters. There were significant positive correlations between Sb, As, Zn, Se, Cd, and Ba, and the correlation coefficients were all greater than 0.68 ($P < 0.05$). The three factors screened explained 49.2%, 36.4%, and 9.5% of the total variance, representing antimony smelting, solid waste pollution, and natural sources, respectively. The findings mentioned above provided valuable references for understanding the heavy metal pollution characteristics in the soil of antimony smelting sites, the biogeochemical behavior of Sb and As, the selection of risk assessment methods, and the application of pollution source identification models. These findings could offer technical support for pollution treatment and resource utilization in antimony smelting sites.

Supplementary Information

The online version contains supplementary material available at https://doi.org/10.1186/s12302-023-00821-5.

Additional file 1: Figure. S1. The study area and the distribution of sampling sites. **Figure. S2.** Single pollution index and Nemerow pollution index of Sb and As in 20 soil samples. **Figure. S3.** Geoaccumulation index of Sb and As in 20 soil samples. **Figure. S4.** BAFs of Sb and As in mugwort plants: **a** Total contents in soils, **b** Chemical fractions (F1+F2+F3) in soils. **Figure. S5.** Non-carcinogenic and carcinogenic risks of HMs in soil using the MEEPRC model. **Figure. S6.** Non-carcinogenic risk of Sb and As in soil: **a** USEPA model, **b** MEEPRC model. **Figure. S7.** Carcinogenic risks of total contents and chemical fractions of As in soils. **Figure. S8.** Correlations coefficients between different HMs in soils. **Table S1.** Exposure factors for dose models. **Table S2.** Reference doses for non-cancer HMs and slope factor for carcinogens.

Acknowledgements
The authors wish to thank the staff of the Environmental Testing and Experiment Center for their help during the sampling and sample analysis process.

Author contributions
L original draft preparation. C review and editing. M methodology and figures. H supervision. Z sample collection and testing. All authors read and approved the final manuscript.

Funding
This work was jointly supported by the National Key R&D Program of China (2020YFC1807703).

Availability of data and materials
The data are not publicly available due to their containing information that could compromise the privacy of the smelter.

Declarations

Ethics approval and consent to participate
Not applicable.

Consent for publication
Not applicable.

Competing interests
The authors declare that they have no known competing financial interests or personal relationships that could have appeared to influence the work reported in this paper.

Received: 8 September 2023 Accepted: 25 November 2023
Published online: 19 December 2023

References

1. Agyeman PC, Kingsley J, Kebonye NM, Khosravi V, Borůvka L, Vašát R (2023) Prediction of the concentration of antimony in agricultural soil using data fusion, terrain attributes combined with regression kriging. Environ Pollut 316:120697
2. Bolan N, Kumar M, Singh E, Kumar A, Singh L, Kumar S, Keerthanan S, Hoang SA, El-Naggar A, Vithanage M, Sarkar B, Wijesekara H, Diyabalanage S, Sooriyakumar P, Vinu A, Wang H, Kirkham MB, Shaheen SM, Rinklebe J, Siddique KHM (2022) Antimony contamination and its risk management in complex environmental settings: a review. Environ Int 158:106908
3. Chen W, Xie T, Li X, Wang R (2018) Thinking of construction of soil pollution prevention and control technology system in China. Acta Pedol Sin 55:557–568
4. CMBQTS (2016) Soil screening levels for environmental risk assessment of sites. DB 50/ T 723–2016. Chongqing municipal bureau of quality and technical supervision, Chongqing
5. CNEMC (1990) The element background values of Chinese soil. China National Environmental Monitoring Centre, Beijing
6. Diquattro S, Castaldi P, Ritch S, Juhasz AL, Brunetti G, Scheckel KG, Garau G, Lombi E (2021) Insights into the fate of antimony (Sb) in contaminated soils: ageing influence on Sb mobility, bioavailability, bioaccessibility and speciation. Sci Total Environ 770:145354
7. Egodawatta LP, Holland A, Koppel D, Jolley DF (2020) Interactive effects of arsenic and antimony on Ipomoea aquatica growth and bioaccumulation in co-contaminated soil. Environ Pollut 259:113830
8. EU (1976) Council Directive 76/464/EEC of 4 May 1976 on pollution caused by certain dangerous substances discharged into the aquatic environment of the community. Official J L 129:23–29
9. Fan M-Y, Zhang Y-L, Lin Y-C, Cao F, Sun Y, Qiu Y, Xing G, Dao X, Fu P (2021) Specific sources of health risks induced by metallic elements in PM2.5 during the wintertime in Beijing. China Atmos Environ 246:118112
10. Fei X, Lou Z, Xiao R, Ren Z, Lv X (2020) Contamination assessment and source apportionment of heavy metals in agricultural soil through the synthesis of PMF and GeogDetector models. Sci Total Environ 747:141293
11. Fu Z, Wu F, Mo C, Deng Q, Meng W, Giesy JP (2016) Comparison of arsenic and antimony biogeochemical behavior in water, soil and tailings from Xikuangshan, China. Sci Total Environ 539:97–104
12. Guo X, Wang K, He M, Liu Z, Yang H, Li S (2014) Antimony smelting process generating solid wastes and dust: Characterization and leaching behaviors. J Environ Sci 26:1549–1556
13. Hakanson L (1980) An ecological risk index for aquatic pollution control.a sedimentological approach. Water Res 14:975–1001
14. Hammel W, Debus R, Steubing L (2000) Mobility of antimony in soil and its availability to plants. Chemosphere 41:1791–1798
15. He M (2007) Distribution and phytoavailability of antimony at an antimony mining and smelting area, Hunan, China. Environ Geochem Health 29:209–219
16. He M, Wang N, Long X, Zhang C, Ma C, Zhong Q, Wang A, Wang Y, Pervaiz A, Shan J (2019) Antimony speciation in the environment: recent advances in understanding the biogeochemical processes and ecological effects. J Environ Sci 75:14–39
17. He Y, Han Z, Wu F, Xiong J, Gu S, Wu P (2021) Spatial distribution and environmental risk of arsenic and antimony in soil around an antimony smelter of Qinglong County. Bull Environ Contam Toxicol 107:1043–1052
18. Jiang H-H, Cai L-M, Hu G-C, Wen H-H, Luo J, Xu H-Q, Chen L-G (2021) An integrated exploration on health risk assessment quantification of

potentially hazardous elements in soils from the perspective of sources. Ecotoxicol Environ Saf 208:111489
19. Li H, Ji H (2017) Chemical speciation, vertical profile and human health risk assessment of heavy metals in soils from coal-mine brownfield, Beijing, China. J Geochem Explor 183:22–32
20. Li J, Huang B, Long J (2021) Effects of different antimony contamination levels on paddy soil bacterial diversity and community structure. Ecotoxicol Environ Saf 220:112339
21. Li J, Wang Q, Oremland Ronald S, Kulp Thomas R, Rensing C, Wang G, Drake HL (2016) Microbial antimony biogeochemistry: enzymes, regulation, and related metabolic pathways. Appl Environ Microbiol 82:5482–5495
22. Li L, Zhang Y, Ippolito JA, Xing W, Qiu K, Yang H (2020) Lead smelting effects heavy metal concentrations in soils, wheat, and potentially humans. Environ Pollut 257:113641
23. Li S, Zhao B, Jin M, Hu L, Zhong H, He Z (2020) A comprehensive survey on the horizontal and vertical distribution of heavy metals and microorganisms in soils of a Pb/Zn smelter. J Hazard Mater 400:123255
24. Li X, Yang H, Zhang C, Zeng G, Liu Y, Xu W, Wu Y, Lan S (2017) Spatial distribution and transport characteristics of heavy metals around an antimony mine area in central China. Chemosphere 170:17–24
25. Li Y, Zhang B, Liu Z, Wang S, Yao J, Borthwick AGL (2020) Vanadium contamination and associated health risk of farmland soil near smelters throughout China. Environ Pollut 263:114540
26. MEEPRC (2018) Soil environmental quality-Risk control standard for soil contamination of development land. GB 36600-2018. Ministry of Ecology and Environment of the People's Republic of China, Beijing
27. MEEPRC (2019) Technical guidelines for risk assessment of soil contamination of land for construction, HJ 25.3-2019. Ministry of Ecology and Environment of the People's Republic of China, Beijing
28. MEPPRC (2015) Solid Waste - Determination of metals - Inductively coupled plasma mass spectrometry (ICP-MS), HJ 766–2015. Ministry of Environmental Protection of the People's Republic of China, Beijing
29. MEPPRC (2016) Soil and sediment-Determination of aqua regia extracts of 12 metal elements-inductively coupled plasma mass spectrometry. HJ 803-2016. Ministry of Environmental Protection of the People's Republic of China, Beijing
30. Mitsunobu S, Harada T, Takahashi Y (2006) Comparison of antimony behavior with that of arsenic under various soil redox conditions. Environ Sci Technol 40:7270–7276
31. Muller G (1979) Schwermetalle in den sedimenten des Rheins-Veranderungen seit 1971. Umschau 79:778–783
32. NHFPCPRC (2016) Determination of multi-elements in foods GB 5009268–2016. National Health and Family Planning Commission of the PRC, Beijing
33. Nishad PA, Bhaskarapillai A (2021) Antimony, a pollutant of emerging concern: a review on industrial sources and remediation technologies. Chemosphere 277:130252
34. Okkenhaug G, Zhu Y-G, He J, Li X, Luo L, Mulder J (2012) Antimony (Sb) and arsenic (As) in Sb mining impacted paddy soil from Xikuangshan, China: differences in mechanisms controlling soil sequestration and uptake in rice. Environ Sci Technol 46:3155–3162
35. Paatero P, Tapper U (1994) Positive matrix factorization: a non-negative factor model with optimal utilization of error estimates of data values. Environmetrics 5:111–126
36. Pan W-S, Zou Q, Hu M, Li W-C, Xiong X-R, Qi Y-T, Wu C (2023) Microbial community composition and cooccurrence patterns driven by co-contamination of arsenic and antimony in antimony-mining area. J Hazard Mater 454:131535
37. Rauret G, López-Sánchez JF, Sahuquillo A, Rubio R, Davidson C, Ure A, Quevauviller P (1999) Improvement of the BCR three step sequential extraction procedure prior to the certification of new sediment and soil reference materials. J Environ Monit 1:57–61
38. Shen Y-W, Zhao C-X, Zhao H, Dong S-F, Xie J-J, Lv M-L, Yuan C-G (2023) Decryption analysis of antimony pollution sources in PM2.5 through a multi-source isotope mixing model based on lead isotopes. Environ Pollut 328:121600
39. USEPA (1979) Water related fate of the 129 priority pollutants. USEPA, Washington
40. USEPA (1989) Risk assessment guidance for superfund. Volume 1: human health evaluation manual (Part A). Office of Emergency and Remedial Response, Washington
41. USEPA (1997) Exposure factors handbook. Office of Research and Development, Washington
42. USEPA (2002) Supplemental guidance for developing soil screening levels for superfund sites, OSWER 9355. Office of Emergency and Remedial Response, Washington
43. Wang H, Zhao Y, Walker TR, Wang Y, Luo Q, Wu H, Wang X (2021) Distribution characteristics, chemical speciation and human health risk assessment of metals in surface dust in Shenyang City. China Appl Geochem 131:105031
44. Wang X, He M, Xie J, Xi J, Lu X (2010) Heavy metal pollution of the world largest antimony mine-affected agricultural soils in Hunan province (China). J Soils Sediments 10:827–837
45. Wang Y, Guo G, Zhang D, Lei M (2021) An integrated method for source apportionment of heavy metal(loid)s in agricultural soils and model uncertainty analysis. Environ Pollut 276:116666
46. Wei X, Zhou Y, Jiang Y, Tsang DCW, Zhang C, Liu J, Zhou Y, Yin M, Wang J, Shen N, Xiao T, Chen Y (2020) Health risks of metal(loid)s in maize (*Zea mays* L.) in an artisanal zinc smelting zone and source fingerprinting by lead isotope. Sci Total Environ 742:140321
47. Wilson SC, Lockwood PV, Ashley PM, Tighe M (2010) The chemistry and behaviour of antimony in the soil environment with comparisons to arsenic: a critical review. Environ Pollut 158:1169–1181
48. Xu L, Dai H, Skuza L, Wei S (2021) Comprehensive exploration of heavy metal contamination and risk assessment at two common smelter sites. Chemosphere 285:131350
49. Xu Q, Shi Y, Qian L, Zhou X, Wang J, Ke L (2022) Tiered ecological risk assessment combined with ecological scenarios for soil in abandoned industrial contaminated sites. J Clean Prod 341:130879
50. Xue S, Korna R, Fan J, Ke W, Lou W, Wang J, Zhu F (2023) Spatial distribution, environmental risks, and sources of potentially toxic elements in soils from a typical abandoned antimony smelting site. J Environ Sci 127:780–790
51. Yang B, Zhou L, Xue N, Li F, Li Y, Vogt RD, Cong X, Yan Y, Liu B (2013) Source apportionment of polycyclic aromatic hydrocarbons in soils of Huanghuai Plain, China: comparison of three receptor models. Sci Total Environ 443:31–39
52. Yuan Y, Xiang M, Liu C, Theng BKG (2017) Geochemical characteristics of heavy metal contamination induced by a sudden wastewater discharge from a smelter. J Geochem Explor 176:33–41
53. Zeng J, Luo X, Cheng Y, Ke W, Hartley W, Li C, Jiang J, Zhu F, Xue S (2022) Corrigendum to "Spatial distribution of toxic metal(loid)s at an abandoned zinc smelting site, Southern China." J Hazard Mater 427:128110
54. Zhang K, Chai F, Zheng Z, Yang Q, Zhong X, Fomba KW, Zhou G (2018) Size distribution and source of heavy metals in particulate matter on the lead and zinc smelting affected area. J Environ Sci 71:188–196
55. Zhao J, Luo Q, Ding L, Fu R, Zhang F, Cui C (2022) Valency distributions and geochemical fractions of arsenic and antimony in non-ferrous smelting soils with varying particle sizes. Ecotoxicol Environ Saf 233:113312
56. Zhong Q, Ma C, Chu J, Wang X, Liu X, Ouyang W, Lin C, He M (2020) Toxicity and bioavailability of antimony in edible amaranth (*Amaranthus tricolor* Linn.) cultivated in two agricultural soil types. Environ Pollut 257:113642
57. Zhou Y, Wang L, Xiao T, Chen Y, Beiyuan J, She J, Zhou Y, Yin M, Liu J, Liu Y, Wang Y, Wang J (2020) Legacy of multiple heavy metal(loid)s contamination and ecological risks in farmland soils from a historical artisanal zinc smelting area. Sci Total Environ 720:137541

Publisher's Note